Towards the Rational Design of MRI Contrast Agents: δ-Substitution of Lanthanide(III) NB-DOTA-Tetraamide Chelates Influences but Does Not Control Coordination Geometry

Christiane E. Carney
Portland State University

Anh D. Tran
University of Texas at Dallas

Jing Wang
University of Texas at Dallas

Matthias C. Schabel
Oregon Health & Science University

A. Dean Sherry
University of Texas at Dallas

Citation Details

Published as: Carney, C. E., Tran, A. D., Wang, J., Schabel, M. C., Sherry, A. D., & Woods, M. (2011). Towards the rational design of MRI contrast agents: δ-substitution of lanthanide(III) NB-DOTA-tetraamide chelates influences but does not control coordination geometry. Chemistry (Weinheim An Der Bergstrasse, Germany), 17(37), 10372–10378. https://doi.org/10.1002/chem.201101007

Authors

Christiane E. Carney, Anh D. Tran, Jing Wang, Matthias C. Schabel, A. Dean Sherry, and Mark Woods

Towards the Rational Design of MRI Contrast Agents: δ-Substitution of Lanthanide(III) NB-DOTA-Tetraamide Chelates Influences but Does Not Control Coordination Geometry[**]

Christiane E. Carney[a], **Anh D. Tran**[b], **Jing Wang**[b], **Matthias C. Schabel**[c], **A. Dean Sherry**[b,d], and **Mark Woods**[a,c]

[a]Department of Chemistry, Portland State University 1719 SW 10th Ave, Portland, OR 97201 (USA) mark.woods@pdx.edu

[b]Department of Chemistry, University of Texas at Dallas 800 W. Campbell Road, Richardson, TX 75080 (USA)

[c]Advanced Imaging Research Center Oregon Health & Science University 3181 S.W. Sam Jackson Park Road, Portland, OR 97239 (USA) woodsmar@ohsu.edu

[d]Advanced Imaging Research Center University of Texas Southwestern Medical Center Harry Hines Blvd., Dallas, TX 75235 (USA)

Abstract

LnDOTA-tetraamide chelates (DOTA=1,4,7,10-tetraazacyclododecane-1,4,7,10-tetraacetic acid) have received considerable recent attention as a result of their potential to act as PARACEST contrast agents for magnetic resonance imaging (MRI). Although PARACEST agents afford several advantages over conventional contrast agents they suffer from substantially higher detection limits; thus, improving the effectiveness of LnDOTA-tetraamide chelates is an important goal. In this study we investigate the potential to extend conformational control of LnDOTA-type ligands to those applicable to PARACEST. Furthermore, the question of whether δ- rather than α-substitution of the pendant arms could be used to control the chelate coordination geometry is addressed. Although δ-substitution does influence coordination geometry it does not afford control. However, it can play an important role in governing the conformation of the amide substituent relative to the chelate in such as way that suggests a PARACEST agent could be designed that has detection limits at least as low as a conventional MRI contrast agent.

Keywords

conformational control; coordination modes; lanthanides; PARACEST agents; water exchange

Introduction

We have recently reported a method by which the coordination geometry adopted by Ln^{3+} chelates of DOTA-type ligands (DOTA=1,4,7,10-tetraazacyclododecane-1,4,7,10-tetraacetic acid) may be selected by appropriate substitution of the pendant arms and macrocyclic ring.[1,2] LnDOTA chelates can interconvert between mono-capped square antiprism (SAP)

Supporting information for this article is available on the WWW under http://dx.doi.org/10.1002/chem.201101007.

and mono-capped twisted square antiprism (TSAP) coordination geometries either by a flip in the conformation of the macrocyclic ring or a reorientation of the pendant arms.[3,4] Substitution can effectively halt these intramolecular processes affording a single coordination geometry.[1,2] The coordination geometry thus obtained is then determined by the relative configuration of the substituents on the macrocyclic ring and the pendant arms; when the configurations at these two locations are the same, a TSAP isomer results and when they are opposed, a SAP isomer results.[1,2] The selection of coordination geometry in this type of chelate is of interest since it may facilitate the design of more effective Gd^{3+}-based MRI contrast agents. TSAP isomers have consistently been found to have water exchange rates that are 50–100-fold faster than those of SAP isomers,[5–7] a critical factor in the behavior of Gd^{3+}-based contrast agents. LnDOTA-tetraamide chelates exhibit a similar coordination chemistry to DOTA chelates but much slower water proton exchange kinetics as a result of the reduced electron density on the central metal ion. These slower exchange rates have sparked interest in this class of chelate as potential PARACEST (paramagnetic chemical exchange saturation transfer) agents.[8,9] Since slow exchange is desirable for PARACEST, SAP isomers are generally preferred. It has been observed that LnDOTA-tetraamides with more bulky amide substituents have a general preference for the SAP coordination geometry, but recent results suggest that changes in the local environment, and in particular the solvent, may cause changes in the coordination chemistry of LnDOTA-tetraamide chelates.[10] Furthermore, addition of a second amide substituent seems to increase the proportion of TSAP isomer present.[10] In light of these observations, we were interested to know whether it was possible to selectively control the coordination geometry of DOTA-tetraamide chelates through substitution in a manner analogous that used for DOTA chelates. Of particular interest was the effect of introducing chirality into the δ-position of an amide substituent of the pendant arm rather than in the α-position as employed previously with DOTA chelates. The motivation for this approach is that α-substitution necessarily involves a synthetic transformation at a chiral center, with all the attendant problems. Control from the δ-position would eliminate these synthetic complications. Chiral amide substituents have been reported to influence both the orientation of pendant arms and configuration at phosphorus in triphosphinate-monoamide chelates.[11] The question we sought to address in this work is whether, in DOTA-tetraamide systems, this approach would not merely influence the orientation of the pendant arms but define it.

Results and Discussion

EuDOTAM-Gly has been widely studied as a potential PARACEST agent[12–14] and, given its potential suitability for use in vivo,[15,16] was therefore an ideal starting point for this investigation. The conformation of the macrocyclic ring was
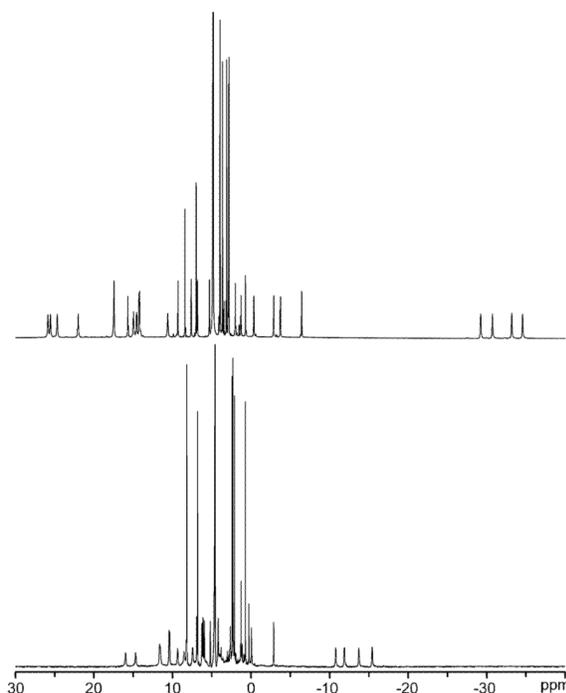
controlled with the same nitrobenzyl substituent employed in our previous systems[1,2]—an *S*- configuration conferring a (δδδδ) conformation upon the macrocyclic ring. Alanine was substituted for glycine in the synthesis of the pendant arms. (*R*)-alanine ethyl ester and (*S*)-alanine benzyl ester were used to prepare the two diastereoisomeric ligands *S-RRRR*-**1** and *S-SSSS*-**1** (Scheme 1). In each case the alanine ester was condensed with bromoacetyl bromide in CH_2Cl_2 with K_2CO_3 as base. The resulting bromoacetamides were then used to alkylate the *S*-2-nitrobenzyl cyclen. Ester cleavage—saponification for the ethyl esters and BCl_3 in CH_2Cl_2 in the case of benzyl esters[17]—afforded *S-RRRR*-**1** and *S-SSSS*-**1**. The Ln^{3+} chelates were then prepared from the corresponding Ln^{3+} triflate in water at pH 6 and purified by preparative RP-HPLC (C18) to afford each chelate in its protonated form.

The coordination geometry of DOTA and DOTA-tetraamide type chelates are known to be strongly affected by the ionic radius of the Ln^{3+} ion. A preference for the TSAP geometry is observed for earlier (larger) Ln^{3+} ions, switching to the SAP geometry as the ionic radius decreases across the series.[18,19] To account for the effect of ionic radius the Pr^{3+}, Eu^{3+}, and Yb^{3+} chelates of each ligand were prepared and examined by ^{1}H NMR spectroscopy. In the case of Pr^{3+}, only one coordination geometry could be detected for each chelate (Figure 1), indicating that, as expected, the *S-RRRR*-isomer adopts the Λ(δδδδ) SAP coordination geometry and the *S-SSSS*-isomer is in the Δ(δδδδ) TSAP conformation, exclusively. Reducing the ionic radius of the Ln^{3+} ion ($Pr^{3+} \rightarrow Eu^{3+} \rightarrow Yb^{3+}$) was found to have no effect on the chelates of *S-RRRR*-**1**, which were found to exist in only one coordination geometry (the Λ(δδδδ) conformation) across the lanthanide series (Figure 1, 2, and 3). In contrast, the chelates of *S-SSSS*-**1** were found to be profoundly affected by changing the ionic radius of the Ln^{3+} ion with increasing amounts of chelate in a SAP coordination geometry being discernable in the NMR spectrum of the Eu^{3+} and Yb^{3+} chelates (Figure 2 and Figure 3). For Eu*S-SSSS*-**1** the amount of SAP isomer observed is quite small, approximately 5%, but for Yb*S-SSSS*-**1** the amount increases to almost 50%. It is also notable that considerable line broadening can be observed in the spectrum of the TSAP isomer of Eu*S-SSSS*-**1**, but not the SAP isomer. The line broadening is also not observed in the corresponding Yb^{3+} chelate. The origin of this effect remains obscure but perhaps relates to an increase in internal

vibrational or torsional motions in the ligand, shortening T_2, as it attempts, but fails, to overcome the energy barrier associated with isomeric exchange.

For a chelate of *S-SSSS-***1** to adopt a SAP coordination geometry, either the macrocyclic ring or the pendant arms must adopt a conformation that opposes the configuration of the chiral center located on that group. A flip in the conformation of the macrocyclic ring would place the nitrobenzyl substituent in an axial position, substantially increasing the torsional strain in the system and may be considered highly unlikely. Rather it seems that the SAP form arises from the pendant arms rotating into the unexpected conformation (Λ rather than Δ for the *S-SSSS*-isomer).[20] In an α-substituted system, torsional strain is minimized by placing the substituent as far from the metal (*trans-* across the N—C$_\alpha$ bond) as possible (Figure 4). This determines the orientation of the pendant arms. The origins of control observed in some δ-substituted systems remain ambiguous; however, a survey of crystallographic data on related systems suggests that a preferred conformation exists.[11,21–27] It appears that the lowest energy conformation points the hydrogen of the chiral center towards the metal ion, the bulkiest substituent is then placed in a pseudo-equatorial position relative to the chelate (Figure 4). This can occur only if the pendant arms are orientated appropriately: Λ for an *R*-configuration, Δ for *S*-configuration. If the arms rotate and adopt the opposite orientation, then the bulky substituent is placed in a pseudo-axial position that is presumably higher in energy (Figure 4). Examples of this situation in the crystallographic literature suggest that this occurs primarily when a second factor forces the arms into the orientation that opposes the configuration of the chiral substituent.[21] It seems likely that the decrease in ionic radius, and perhaps the associated increase in charge density, contributes to an increase in this second factor for Ln*S-SSSS-***1** chelates as one passes along the Ln^{3+} series. All LnDOTAM-Gly chelates exhibit an exclusive preference for the SAP geometry and although the reasons for this are unclear, it does explain why no TSAP isomer was observed for any of the Ln*S-RRRR-***1** chelates, even for Pr^{3+} which often exhibits a preference for this co-ordination geometry. This phenomenon, which drives LnDOTAM-Gly chelates into exclusively SAP geometries, is presumably the same as that which results in SAP isomers being observed for the Ln*S-SSSS-***1** chelates. The SAP isomer that is observed would be the same Λ(δδδδ) conformation observed for the Ln*S-RRRR-***1** chelates but with one significant difference: the carboxylate substituent must occupy a pseudo-axial rather than a pseudo-equatorial position.

Although the substitution of the δ-position does not afford control over the coordination geometry in Ln*S-SSSS-***1** chelates, preliminary results suggest that the intramolecular exchange processes between the two coordination geometries have been "frozen out". No evidence of exchange could be detected by EXSY or by saturation transfer experiments on the highly shifted acetate peaks of Yb*S-SSSS-***1**, suggesting that the two isomers (SAP and TSAP) are either not in exchange or exchange so slowly that the process cannot be detected by these techniques.

From the point of view of PARACEST agent design, chelates that adopt a SAP coordination geometry are preferred because, in general, they possess slower water proton exchange kinetics. The unexpected appearance of a second conformer of the SAP coordination geometry, that adopted by Eu*S-SSSS-***1**, afforded a unique opportunity to examine how the orientation of the carboxylate group affects CEST. NMR samples were prepared to compare the CEST of Eu*S-RRRR-***1** with that of Eu*S-SSSS-***1** at 1) the same overall concentration of chelate (274 μm) and 2) the same concentration of SAP isomer (13.7 μm) (Figure 5). CEST peaks at approximately + 50 ppm were observed for both chelates: 52 ppm for Eu*S-RRRR-***1** and 49 ppm for Eu*S-SSSS-***1**, consistent with CEST arising from a SAP coordination geometry in each case. When the overall chelate concentration ([Eu^{3+}]) is the same, the magnitude of CEST arising from Eu*S-RRRR-***1** is approximately threefold greater than that

of Eu*S-SSSS*-**1** (Figure 5, open symbols), but the SAP isomer constitutes only 1/20 of the Eu*S-SSSS*-**1** chelate. When the concentrations of the SAP isomer in each sample were normalized ([SAP]=13.7 µm), no CEST was observed from Eu-*S-RRRR*-**1**, whereas Eu*S-SSSS*-**1** produces a change in bulk water signal of approximately 10% (Figure 5, circles). Clearly the SAP isomer of Eu*S-SSSS*-**1** is a substantially more effective PARACEST agent than that of Eu*S-RRRR*-**1**.

To better understand the difference between these two SAP isomers these CEST data were quantitatively analyzed. In general CEST spectra may be fitted to the Bloch equation modified for exchange,[28] however, a reasonable fit between this model and the data for Eu*S-SSSS*-**1** could not be obtained when the concentration of water shifted to +49 ppm was the same as that of the SAP isomer (see Figure S2 in the Supporting Information). The water proton residence lifetime (τ_M^H) for the SAP isomer of each chelate was therefore determined independently by the so-called ω-method',[29] affording values of τ_M^H=116 µs (Eu*S-RRRR*-**1**) and 65 µs (Eu*S-SSSS*-**1**) (Figure 6). These values could then be applied to modeling the data to the modified Bloch equations. The spectrum of Eu-*S-RRRR*-**1** fitted to theory satisfactorily (Figure 5), however, the spectrum of Eu*S-SSSS*-**1** continued to prove difficult to fit. A satisfactory fit for these data could only be obtained when the concentration of protons in the highly shifted pool (+49 ppm) was allowed to increase beyond the concentration of the SAP isomer. When the concentration of water molecule in this pool was 3.7 times that of the SAP isomer a good fit was obtained suggesting that between two and three additional water molecules may be present in the highly shifted pool of Eu*S-SSSS*-**1** (Figure 5). These additional water molecules must be closely held and highly shifted by Eu^{3+}, although perhaps not so highly shifted as the coordinated water, which may account for the slightly smaller shift of the CEST peak in this chelate. These additional water protons would certainly explain why the SAP isomer of Eu*S-SSSS*-**1** is a much more effective PARACEST agent than Eu*S-RRRR*-**1**.

Although two conformational isomers (pseudo-axial/equatorial) have been postulated previously[11] the two diastereoisomeric chelates of Eu**1** have for the first time afforded an opportunity to examine the CEST properties of each. The *S-SSSS* (pseudo-axial) isomer is a significantly more effective PARACEST agent possibly because it closely holds more than one water molecule in a highly shifted pool. In such a situation the value of τ_M^H reflects all protons in this pool, it is therefore difficult to understand exactly how the exchange kinetics of these chelates modulate CEST.

These results demonstrate, for the first time, that it may be possible to design PARACEST agents that have detection limits for MRI comparable to current MRI contrast agents. In Figure 4 Eu*S-SSSS*-**1** generates about 10% CEST at an overall chelate concentration of 0.274 mM. However, only about 5% of the chelate is responsible for this CEST so the active concentration is just 13.7 µm, but these measurements are in only 10% water in acetonitrile. Assuming a linear relationship between CEST and concentration (which is approximately true at very low concentrations),[30] 137 µm could generate 10% CEST. A change in water signal intensity of only about 3% is required to observe contrast changes in an MR image, so just 46 µm of the SAP isomer of Eu*S-SSSS*-**1** should afford an MRI detectable level of CEST in pure water.

Although these measurements were performed by using admittedly high B_1 powers (upwards of 1 kHz) there is scope for B_1 to be substantially reduced before the detection limit of the active form of this agent exceeds 0.1 mM, the typical dose of a clinical MRI contrast agent (0.1 mmol kg^{-1}). Clearly further experimentation is required to better understand the potential of the type of system for PARACEST design. Nonetheless, these preliminary data do suggest that attending to the coordination chemistry of LnDOTA-

tetraamide chelates may provide a means by which the detection limit problem in CEST may be overcome.

Experimental Section

General remarks

All solvents and reagents were purchased from commercial sources and used as received except where noted. 'Water' refers to deionized water with a resistivity of <18.2 MΩcm. ^{1}H and ^{13}C NMR spectra were acquired on a JOEL Eclipse 270 spectrometer operating at 270.17 and 67.94 MHz, respectively. CEST spectra were acquired on a Bruker Avance IIa 400 spectrometer operating at 400.13 MHz. Infrared spectra were recorded on a Nicolet Avatar 360 FTIR spectrophotometer. Melting points were recorded on a Fisher–Johns melting point apparatus and are uncorrected. RP-HPLC purification was performed on a Waters δ-prep HPLC system using a 30×250 mm Phenomenex Luna C18(2) column. In all cases ligands were purified by eluting for 5 min of 100% water (0.037% HCl) followed by a linear gradient over 35 min to 40% acetonitrile and 60% water (0.037% HCl) at a flow rate of 30 mL min^{-1}. Chelates were purified by eluting for 5 min with 100% water (0.037% HCl) followed by a linear gradient over 35 min to 10% acetonitrile and 90% water (0.037% HCl) at a flow rate of 30 mL min^{-1}. Elution of products was monitored by UV absorbance at 210 and 270 nm.

(*R*)-*N*-(Ethyl-2-propionate) bromoacetamide (2)

To a solution of bromoacetyl bromide (2.40 mL, 26.3 mmol) in dichloromethane (100 mL) was added potassium carbonate (6.04 g, 43.8 mmol) and the resulting suspension was cooled to 0°C. A solution of (*R*)-alanine ethyl ester (2.57 g, 21.9 mmol) in dichloromethane (50 mL) was added dropwise over a period of 20 min. The mixture was stirred for a further 30 min at 0°C and 18 more hours at room temperature. Water (30 mL) was added cautiously and the two layers separated. The aqueous phase was extracted with dichloromethane (50 mL), the organic phases were combined, dried (Na$_2$SO$_4$), and the solvents removed under reduced pressure. The residue was taken up into a minimum of dichloromethane and recrystallized by addition ethyl ether and hexanes at −20°C to afford a colorless solid (1.98 g 38%). M.p. 66–67°C; ^{1}H NMR (CDCl$_3$, 270 MHz): δ=7.13 (s br, 1H, NH), 4.52 (dq, $^3J_{HH}$=7 Hz, $^3J_{HH}$=7 Hz, 1H, NHC*H*CH$_3$), 4.26 (q, $^3J_{HH}$=8 Hz, 2H, OC*H*$_2$CH$_3$), 3.82 (s, 2H, BrCH$_2$), 1.45 (d, $^3J_{HH}$=7 Hz, 3H, CHC*H*$_3$), 1.27 ppm (t, $^3J_{HH}$=8 Hz, 3H, CH$_2$C*H*$_3$); ^{13}C NMR (CDCl$_3$, 68 MHz): δ=171.6 (C=O), 164.5 (NHC=O), 60.1 (OCH$_2$), 47.8 (BrCH$_2$), 27.6 (CH), 17.3 (OCH$_2$CH$_3$), 13.4 ppm (CHCH$_3$); ν$_{max}$ (KBr disc)=3743 (NH), 1738 (CO$_2$), 1647 cm^{-1} (NHC=O); *m/z* (ESMS EI−): 236 (100%, [*M*−H$^+$]$^-$), appropriate isotope patterns were observed.

(*S*)-*N*-(Benzyl-2-propionate) bromoacetamide (3)

$_L$-Alanine benzyl ester hydrochloride (4.0 g, 18.5 mmol) was dissolved in water (20 mL) and sodium carbonate added until the solution pH exceeded 12. The solution was then extracted with dichloromethane (2×200 mL). The organic extracts were combined, dried (Na$_2$SO$_4$), and the solvents were removed under reduced pressure. The residue was taken up into dichloromethane (50 mL) and the resulting solution added dropwise to a solution of bromoacetyl bromide (2.0 mL, 22.2 mmol) in dichloromethane (100 mL) containing potassium carbonate (5.11 g, 37.0 mmol) and cooled to 0°C in an ice-bath. Addition was carried out over a period of 20 min and the reaction stirred for a further 30 min at 0°C. The reaction mixture was allowed to warm to room temperature and stirred for 18 h at ambient temperature. Water (30 mL) was added cautiously and the two layers separated. The aqueous phase was extracted with dichloromethane (50 mL), the organic phases were combined, dried (Na$_2$SO$_4$), and the solvents removed under reduced pressure. The residue

was taken up into a minimum of dichloromethane and recrystallized by addition ethyl ether and hexanes at −20°C to afford a colorless solid (3.44 g, 62%). M.p. 59–61°C; ^{1}H NMR (CDCl₃, 270 MHz): δ=7.34 (m, 5H, Ar), 7.06 (s br, 1H, NH), 5.12 (d, $^2J_{HH}$=10 Hz, 1H, aa' system, ArCH₂) 5.11 (d, $^2J_{HH}$=10 Hz, 1H, aa system, ArCH₂), 4.6 (dq, $^3J_{HH}$=7 Hz, $^3J_{HH}$=7 Hz, 1H, NHCHCH₃), 3.82 (s, 2H, BrCH₂), 1.47 ppm (d, $^3J_{HH}$=7 Hz, 3H, CH₃); ^{13}C NMR (CDCl₃, 68 MHz): δ=172.4 (CO₂), 165.6 (NHC=O), 135.2 (Ar), 129.9 (Ar), 129.1 (Ar), 128.4 (Ar), 67.7 (ArCH₂), 49.2 (BrCH₂), 29.4 (CH), 18.7 ppm (CH₃); ν_{max} (KBr disc): 1734 (CO₂), 1717 (CO₂), 1653 cm^{-1} (NHC=O); m/z (ESMS EI−): 298 (100%, [M−H$^+$]$^−$) an appropriate isotope pattern was observed.

(1R, 4R, 7R, 10R)-δ, δ′, δ″, δ‴-Tetramethyl-[2-(S)-(p-nitrobenzyl)-1,4,7,10-tetraazacyclododecane]-1,4,7,10-tetraacetateacetamide (H₄S-$RRRR$-1)

2-S-(p-Nitrobenzyl) cyclen (150 mg, 0.49 mmol) and the bromoacetamide **2** (581 mg, 2.44 mmol) were dissolved in acetonitrile (30 mL), and potassium carbonate (337 mg, 2.44 mmol) was added. The resulting suspension was heated under reflux with stirring for seven days. The solvents were then removed under reduced pressure and the residue taken up into water (20 mL) and dichloromethane (100 mL). The two layers were separated and the aqueous phase extracted with dichloromethane (2×50 mL). The organic phases were combined, dried (Na₂SO₄), and the solvents removed under reduced pressure. The residue was taken up into tetrahydrofuran (5 mL) and water (10 mL) and a 1ₘ sodium hydroxide solution (2.4 mL) added. The resulting monophasic solution was heated to 60°C for 48 h. The solvents were removed under reduced pressure and the residue taken up into water and the pH adjusted to 7 with HCl prior to RP-HPLC purification. After lyophilization of the solvents the dihydrochloride salt of title compound was obtained as a colorless solid (147 mg, 30%). R$_T$=27.79 min; m.p.>170°C; ^{1}H NMR (D₂O, 270 MHz): δ=8.11 (d, $^3J_{HH}$=8 Hz, 2H, Ar), 7.40 (d, $^3J_{HH}$=8 Hz, 2H, Ar), 2.66–4.43 (m br, 29H, ring NCH₂, CH₂C=O, CH₂Ar, CHCH₃), 1.31 ppm (m, 12H, CHCH₃); m/z (ESMS EI+): 824 (100%, [M+H$^+$]); ν_{max} (iTR): 3023 (NH), 1733 (CO₂), 1656 (C=ONH), 1546, 1519, 1454, 1346, 1210, 1157, 943, 735 cm^{-1}.

(1S, 4S, 7S, 10S)-δ, δ′, δ″, δ‴-Tetramethyl-[2-(S)-(p-nitrobenzyl)-1,4,7,10-tetraazacyclododecane]-1,4,7,10-tetraacetateacetamide (H₄S-$SSSS$-1)

2-S-(p-Nitrobenzyl) cyclen (250 mg, 0.81 mmol) and the bromoacetamide **3** (1.22 g, 4.07 mmol) were dissolved in acetonitrile (30 mL), and potassium carbonate (562 mg, 4.07 mmol) was added. The resulting suspension was heated under reflux with stirring for seven days. The solvents were then removed under reduced pressure and the residue taken up into water (20 mL) and dichloromethane (100 mL). The two layers were separated and the aqueous phase extracted with dichloromethane (2×50 mL). The organic phases were combined, dried (Na₂SO₄), and the solvents removed under reduced pressure. The residue was taken up into dry chloroform (10 mL); 5 mL of the resulting solution was transferred to a reaction flask which was purged with argon. The reaction mixture was cooled to −10°C in a salt/ice-bath, and a 1ₘ solution of BCl₃ in dichloromethane (1.6 mL) was added. After addition the reaction mixture was allowed to warm to ambient temperature and was then stirred for 14 h. Water (2 mL) was added dropwise to quench the reaction, followed by 1ₘ HCl (8 mL) and the ligand was extracted into the aqueous phase. The ligand solution was used directly to purify the title compound by RP-HPLC. After lyophilization of the solvents the dihydrochloride salt of title compound was obtained as a colorless solid (78.4 mg, 20%). R$_T$=25.94 min; m.p.>170°C; ^{1}H NMR (D₂O, 270 MHz): δ=8.21 (d, $^3J_{HH}$=8 Hz, 2H, Ar), 7.42 (d, $^3J_{HH}$=8 Hz, 2H, Ar), 2.72–4.31 (m br, 29H, ring NCH₂, CH₂C=O, CH₂Ar, CHCH₃), 1.28 ppm (m, 12H, CHCH₃); m/z (ESMS EI+): 824 (100%, [M+H$^+$]$^+$); ν_{max} (iTR): 3169 (NH), 1727 (CO₂), 1617 (C=ONH), 1455, 1346, 1253, 1155, 957, 821, 751 cm^{-1}.

General procedure for the preparation of Ln³⁺ chelates

Europium triflate (15 mg, 24.6 mmol) and **1** (20 mg, 22.3 mmol) were dissolved in water and the pH adjusted to 6 by addition of NaOH (1$_M$ aqueous solution). The resulting solution was heated at 60 C for 24 h and then allowed to cool to room temperature. After filtration through a 20 mm syringe filter the reaction mixed was injected directly onto a preparative HPLC system for purification. Chelates were obtained by lyophilization of the fraction containing the major reaction product.

Praseodymium(III) (1*R*, 4*R*, 7*R*, 10*R*)-δ, δ′, δ″, δ‴-Tetramethyl-[2-(*S*)-(p-nitrobenzyl)-1,4,7,10-tetraazacyclododecane]-1,4,7,10-tetraacetateacetamide (HPr*S*-*RRRR*-1)

R_T=30.20 min; *m/z* (ESMS EI−): 963 (100%, [*M*−H⁺]⁻) an appropriate isotope pattern was observed.

Europium(III) (1*R*, 4*R*, 7*R*, 10*R*)-δ, δ′, δ″, δ‴-Tetramethyl-[2-(*S*)-(*p*-nitrobenzyl)-1,4,7,10-tetraazacyclododecane]-1,4,7,10-tetraacetateacetamide (HEu*S*-*RRRR*-1)

R_T=24.96 min; *m/z* (ESMS EI−): 975 (100%, [*M*−H⁺]⁻) an appropriate isotope pattern was observed.

Ytterbium(III) (1*R*, 4*R*, 7*R*, 10*R*)-δ, δ′, δ″, δ‴-Tetramethyl-[2-(*S*)-(*p*-nitrobenzyl)-1,4,7,10-tetraazacyclododecane]-1,4,7,10-tetraacetateacetamide (HYb*S*-*RRRR*-1)

R_T=31.31 min; *m/z* (ESMS EI−): 996 (100%, [*M*−H⁺]⁻) an appropriate isotope pattern was observed.

Praseodymium(III) (1*S*, 4*S*, 7*S*, 10*S*)-δ, δ′, δ″, δ‴-Tetramethyl-[2-(*S*)-(*p*-nitrobenzyl)-1,4,7,10-tetraazacyclododecane]-1,4,7,10-tetraacetateacetamide (HPr*S*-*SSSS*-1)

R_T=25.33 min; *m/z* (ESMS EI−): 963 (100%, [*M*−H⁺]⁻) an appropriate isotope pattern was observed.

Europium(III) (1*S*, 4*S*, 7*S*, 10*S*)-δ, δ′, δ″, δ‴-Tetramethyl-[2-(*S*)-(*p*-nitrobenzyl)-1,4,7,10-tetraazacyclododecane]-1,4,7,10-tetraacetateacetamide (HEu*S*-*SSSS*-1)

R_T=30.24 min; *m/z* (ESMS EI−): 975 (100%, [*M*−H⁺]⁻) an appropriate isotope pattern was observed.

Ytterbium(III) (1*S*, 4*S*, 7*S*, 10*S*)-δ, δ′, δ″, δ‴-Tetramethyl-[2-(*S*)-(*p*-nitrobenzyl)-1,4,7,10-tetraazacyclododecane]-1,4,7,10-tetraacetateacetamide (HYb*S*-*SSSS*-1)

R_T=20.45 min; *m/z* (ESMS EI−): 996 (100%, [*M*−H⁺]⁻) an appropriate isotope pattern was observed.

CEST fitting

CEST spectra were recorded at six different B_1 powers for each chelate: 42.7 μT, 36.3 μT, 34.3 μT, 30.1 μT, 27.4 μT, and 24.3 μT (see Figure S1 in the Supporting Information). The water proton exchange kinetics for each SAP isomer were determined by plotting the magnetization at the CEST peak minimum as a function of the initial magnetization ($M_Z/(M_0−M_Z)$) against the reciprocal of the square of the B_1 power expressed in rad s⁻¹ (1 ω^2) (Figure 6). The data were then fitted by using linear regression analysis and the intercept of the line with the *x* axis provides the water exchange rate directly.[29]

The CEST spectra were then fitted to the Bloch equations modified for exchange as previously described.[28] A 2-pool model was used to fit the data for Eu*S*-*RRRR*-**1**

representing the bulk water pool, the bound or shifted water pool. The inclusion of a pool for the amide protons was found not to affect the fitting and therefore excluded from the all fitting models. A 3-pool model was used to fit the data for Eu*S-RRRR*-**1** representing the bulk water, the bound water or shifted water associated with the SAP isomer and the bound or shifted water associated with the TSAP isomer.

The pre-saturation power (B_1) was held fixed during fitting. The water proton exchange lifetime (τ_M^H) was constrained to lie within 10% of the value determined by the ω-fitting. In initial fittings the concentration of each pool was deconstrained to reflect the confidence level of the concentration determination. T_1 values for the bulk water pool were determined experimentally using an inversion recovery pulse sequence and held fixed during fitting. T_1 values for the other pools could not be determined by direct measurement owing to the low chelate concentrations of each sample. The T_1s of these pools and all T_2 values were allowed to float over the range of values previously found in CEST fitting routines in EuDOTA-tetramide chelates.[31] The value of τ_M^H for the TSAP isomer, which does appear to influence the shape of the direct saturation peak at 0 ppm (witness the downfield edge of the peak), was constrained to have a ratio of between 1/40 and 1/60 of the τ_M^H value of the SAP isomer. This ratio is consistent with previously reported behavioral patterns in this type of chelate.

Fitting the CEST data acquired at B_1=1282.8 Hz afforded a good fit to the data for Eu*S-RRRR*-**1**. However, a suitable fit to the *S-SSSS*-isomer could not be obtained when the concentration was constrained as described (see Figure S2 in the Supporting Information). Only when the concentration of the highly shifted pool is allowed to float and fit to values 3.7 times higher than the 13.7 μm chelate concentration is an adequate fit achieved.

Supplementary Material

Refer to Web version on PubMed Central for supplementary material.

Acknowledgments

References

[1]. Woods M, Kovacs Z, Zhang S, Sherry AD. Angew. Chem. 2003; 115:6069.Angew. Chem. Int. Ed. 2003; 42:5889.

[2]. Woods M, Botta M, Avedano S, Wang J, Sherry AD. Dalton Trans. 2005:3829. [PubMed: 16311635]

[3]. Aime S, Botta M, Ermondi G. Inorg. Chem. 1992; 31:4291.

[4]. Hoeft S, Roth K. Chem. Ber. 1993; 126:869.

[5]. Aime S, Barge A, Bruce JI, Botta M, Howard JAK, Moloney JM, Parker D, de Sousa AS, Woods M. J. Am. Chem. Soc. 1999; 121:5762.

[6]. Dunand FA, Aime S, Merbach AE. J. Am. Chem. Soc. 2000; 122:1506.

[7]. Woods M, Aime S, Botta M, Howard JAK, Moloney JM, Navet M, Parker D, Port M, Rousseaux O. J. Am. Chem. Soc. 2000; 122:9781.

[8]. Woods M, Woessner DE, Sherry AD. Chem. Soc. Rev. 2006; 35:500. [PubMed: 16729144]

[9]. Zhang S, Winter P, Wu K, Sherry AD. J. Am. Chem. Soc. 2001; 123:1517. [PubMed: 11456734]

[10]. Miller KJ, Saherwala AA, Webber BC, Wu Y, Sherry AD, Woods M. Inorg. Chem. 2010; 49:8662. [PubMed: 20812752]

[11]. Aime S, Botta M, Dickins RS, Maupin CL, Parker D, Riehl JP, Williams JAG. J. Chem. Soc. Dalton Trans. 1998:881.

[12]. Baranyai Z, Brücher E, Ivanyi T, Kiraly R, Lazar I, Zekany L. Helv. Chim. Acta. 2005; 88:604.

[13]. Terreno E, Daniela D. Castelli, Cravotto G, Milone L, Aime S. Invest. Radiol. 2004; 39:235. [PubMed: 15021328]

[14]. Zhang S, Malloy CR, Sherry AD. J. Am. Chem. Soc. 2005; 127:17572. [PubMed: 16351064]

[15]. Woods M, Caravan P, Geraldes CFGC, Greenfield MT, Kiefer GE, Lin M, McMillan K, Prata MIM, Santos AC, Sun X, Wang J, Zhang S, Zhao P, Sherry AD. Invest. Radiol. 2008; 43:861. [PubMed: 19002058]

[16]. Sherry AD, Caravan P, Lenkinski RE. J. Magn. Reson. Imaging. 2009; 30:1240. [PubMed: 19938036]

[17]. Schmidt U, Kroner M, Griesser H. Synthesis. 1991:294.

[18]. Aime S, Botta M, Fasano M, Marques MPM, Geraldes CFGC, Pubanz D, Merbach AE. Inorg. Chem. 1997; 36:2059. [PubMed: 11669824]

[19]. Vipond J, Woods M, Zhao P, Tircso G, Ren JM, Bott SG, Ogrin D, Kiefer GE, Kovacs Z, Sherry AD. Inorg. Chem. 2007; 46:2584. [PubMed: 17295475]

[20]. Mani T, Tircso G, Zhao P, Sherry AD, Woods M. Inorg. Chem. 2009; 48:10338. [PubMed: 19799440]

[21]. Dickins RS, Batsanov AS, Howard JAK, Parker D, Puschmann H, Salamano S. Dalton Trans. 2004:70. [PubMed: 15356744]

[22]. Dickins RS, Howard JAK, Moloney JM, Parker D, Peacock RD, Siligardi G. Chem. Commun. 1997:1747.

[23]. Dickins RS, Howard JAK, Lehmann CW, Moloney J, Parker D, Peacock RD. Angew. Chem. 1997; 109:541.Angew. Chem. Int. Ed. Engl. 1997; 36:521.

[24]. Dickins RS, Howard JAK, Maupin CL, Moloney JM, Parker D, Riehl JP, Siligardi G, Williams JAG. Chem. Eur. J. 1999; 5:1095.

[25]. Dickins RS, Aime S, Batsanov AS, Beeby A, Botta M, Bruce JI, Howard JAK, Love CS, Parker D, Peacock RD, Puschmann H. J. Am. Chem. Soc. 2002; 124:12697. [PubMed: 12392417]

[26]. Gunnlaugsson T, Davies RJH, Nieuwenhuyzen M, O'Brien JE, Stevenson CS, Mulready S. Polyhedron. 2003; 22:711.

[27]. Thompson AL, Parker D, Fulton DA, Howard JAK, Pandya SU, Puschmann H, Senanayake K, Stenson PA, Badari A, Botta M, Avedano S, Aime S. Dalton Trans. 2006:5605. [PubMed: 17225897]

[28]. Woessner DE, Zhang S, Merritt ME, Sherry AD. Magn. Reson. Med. 2005; 53:790. [PubMed: 15799055]

[29]. Dixon WT, Ren J, Lubag AJM, Ratnakar J, Vinogradov E, Hancu I, Lenkinski RE, Sherry AD. Magn. Reson. Med. 2010; 63:625. [PubMed: 20187174]

[30]. Wu Y, Zhou Y, Ouari O, Woods M, Zhao P, Soesbe TC, Kiefer GE, Sherry AD. J. Am. Chem. Soc. 2008; 130:13854. [PubMed: 18817395]

[31]. Woods M, Woessner DE, Zhao P, Pasha A, Yang M-Y, Huang C-H, Vasalitiy O, Morrow JR, Sherry AD. J. Am. Chem. Soc. 2006; 128:10155. [PubMed: 16881645]
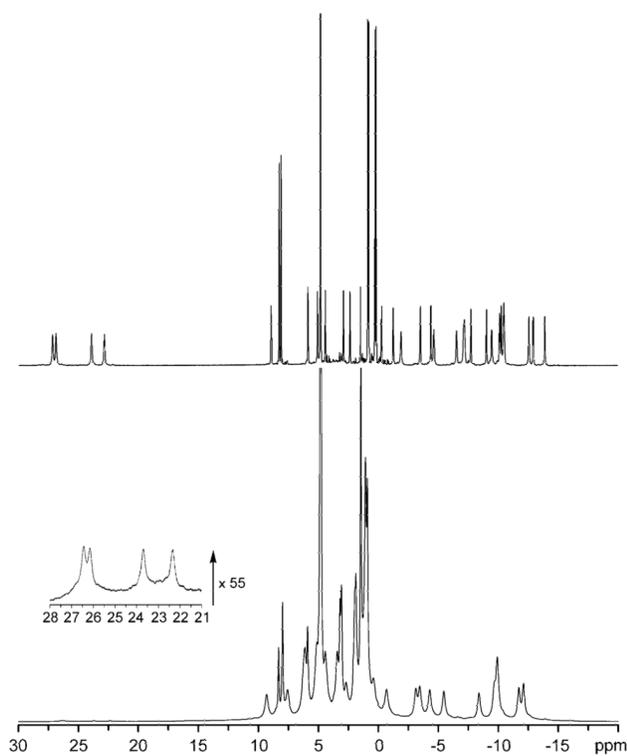
Scheme 1.
The preparation of the two diastereoisomeric ligands **1**. Reagents and conditions: *S-RRRR*-**1**, R=Et: i. BrCH$_2$COBr/K$_2$CO$_3$/CH$_2$Cl$_2$/0°C; ii. *S*-NB-cyclen/K$_2$CO$_3$/MeCN/60°C; iii. NaOH/ H$_2$O/THF; iv. HCl: *S-SSSS*-**1**, R=Bn: i. BrCH$_2$COBr/K$_2$CO$_3$/CH$_2$Cl$_2$/0°C; ii. *S*-NB-cyclen/ K$_2$CO$_3$/MeCN/60°C; iii. BCl$_3$/CH$_2$Cl$_2$/THF; iv. H$_2$O.
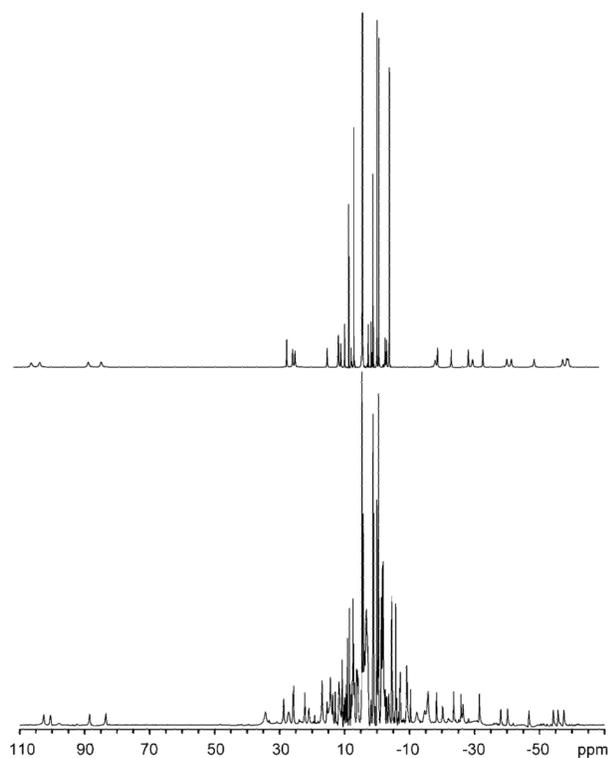
Figure 1.
The ^{1}H NMR spectra of Pr*S-RRRR*-**1** (top) Pr*S-SSSS*-**1** (bottom) and recorded at 400 MHz and 300 K in D$_2$O at pD 4. The four highly shifted peaks between δ=−28 and −35 ppm (top) and δ=−10 and −16 ppm (bottom), are characteristic of the shifts of the *ax*^{S} protons in SAP and TSAP isomers of PrDOTA-tetraamide chelates, respectively.
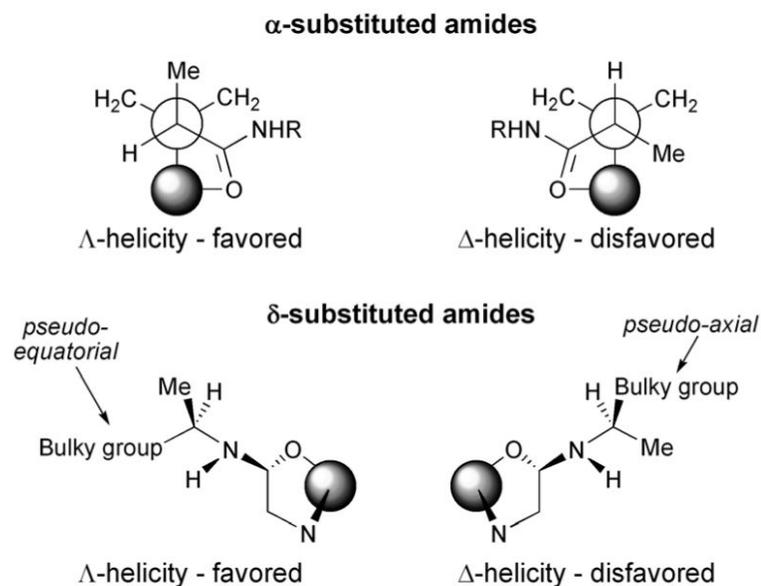
Figure 2.
The ^{1}H NMR spectra of Eu*S-RRRR*-**1** (top), Eu*S-SSSS*-**1** (bottom) recorded at 400 MHz and 300 K in D$_2$O at pD 4. The four shifted peaks between 22 and 27 ppm (both spectra) and 7 and 10 ppm (bottom) are typical of those observed for the SAP and TSAP isomers of EuDOTA-tetraamide chelates, respectively.
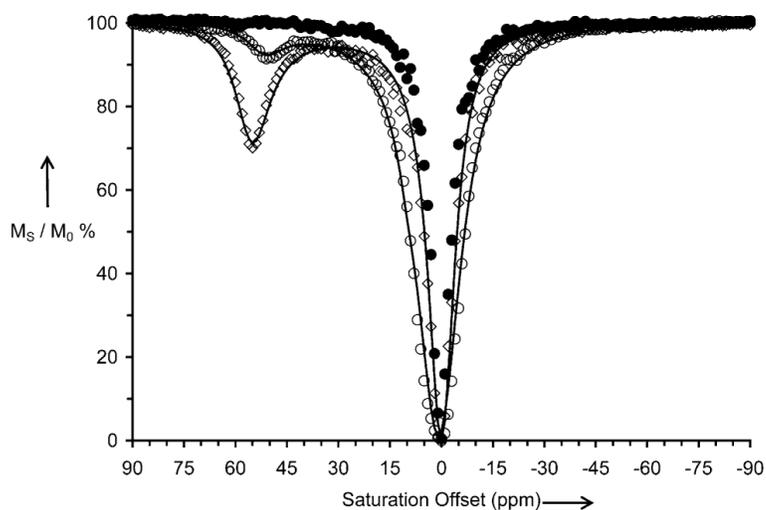
Figure 3.
The ^{1}H NMR spectra of Yb*S-RRRR*-**1** (top), Yb*S-SSSS*-**1** (bottom) recorded at 400 MHz and 275 K in D$_2$O at pD 4. The four shifted peaks between 82 and 103 ppm (both spectra) and 20 and 35 ppm (bottom) are typical of those observed for the SAP and TSAP isomers of YbDOTA-tetraamide chelates, respectively.
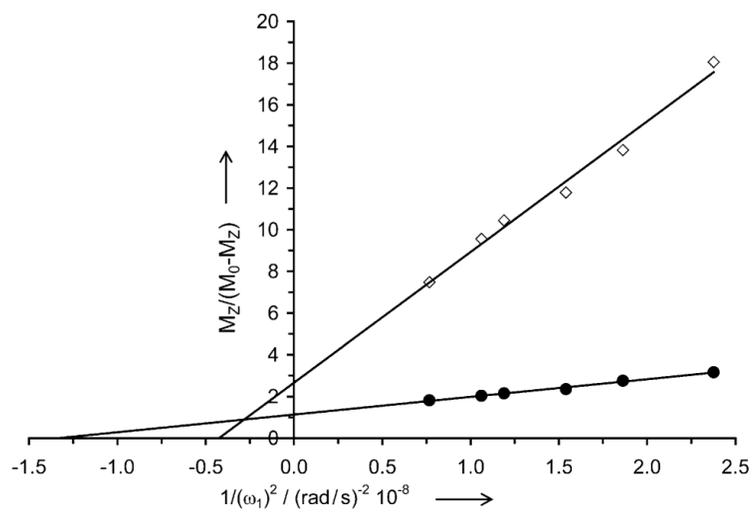
Figure 4.
The orientation of chiral pendant arms and how they are affected by α- (top) and δ-substitution (bottom), in each case the configuration at carbon is *R*.
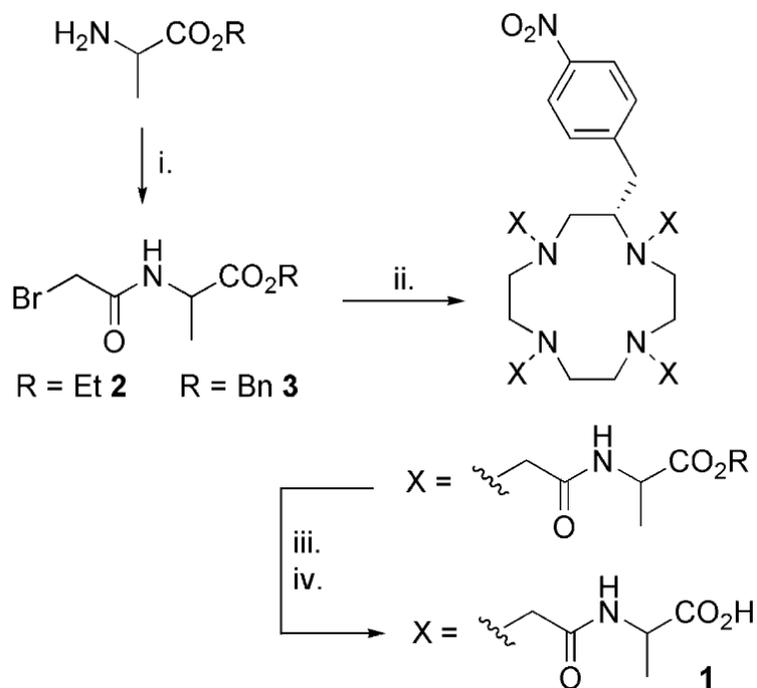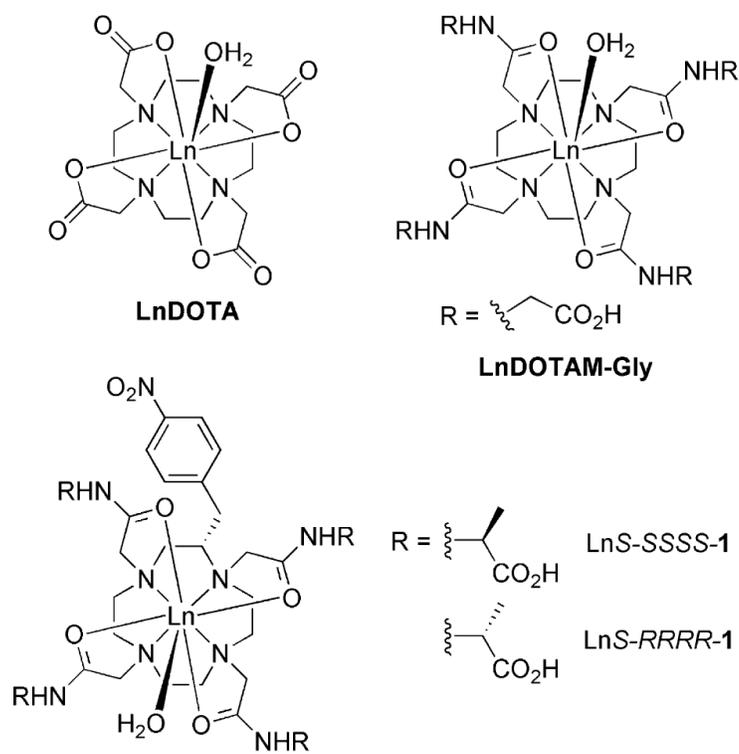
Figure 5.
CEST spectra of solutions of EuS-*RRRR*-**1** ([Eu^{3+}]=[SAP]=274 μ$_M$ open diamonds; [Eu^{3+}]=[SAP]=13.7 μ$_M$ closed circles) and EuS-*SSSS*-**1** ([Eu^{3+}]=274 μ$_M$, [SAP]=13.7 μ$_M$ open circles) in CD$_3$CN (10% H$_2$O) recorded at 400 MHz; 298 K; irr. time=10 s; B$_1$=30 μT.

Figure 6.
The ω-plots of Eu*S-RRRR*-**1** (filled circles) and Eu*S-SSSS*-**1** (open diamonds), data taken from the CEST spectra in Figure S1 in the Supporting Information. The difference in slope of the two lines can be attributed to the difference in SAP isomer concentration between the two samples. The water proton residence lifetimes are afforded by the intercept of the *x* axis.